Science Advances
AAAS

advances.sciencemag.org/cgi/content/full/4/7/eaat9457/DC1

Supplementary Materials for

Phase control in a spin-triplet SQUID

Joseph A. Glick, Victor Aguilar, Adel B. Gougam, Bethany M. Niedzielski, Eric C. Gingrich, Reza Loloee, William P. Pratt Jr., Norman O. Birge*

*Corresponding author. Email: birge@pa.msu.edu

Published 27 July 2018, *Sci. Adv.* **4**, eaat9457 (2018)
DOI: 10.1126/sciadv.aat9457

This PDF file includes:

Additional Low-Temperature Measurements

As shown in Fig. 3 of the main text, and discussed further in the Material and Methods section, the small critical currents of the SQUIDs studied in this work lead to significant rounding of the I-V curves. That rounding is caused by fluctuations in the electromagnetic environment of the junctions, due either to temperature, the measurement apparatus, or interference from sources external to the cryostat. Such fluctuations not only cause rounding, but they may also decrease the amplitude of the critical current extracted from the fitting procedure. While the qualitative conclusions of this work are immune to such considerations, the quantitative accuracy of the analysis is not. To ascertain the extent to which external interference may have influenced the maximum measured critical currents of our SQUIDs, we measured one sample in a variable-temperature cryostat with heavily filtered electrical lines. That cryostat is not equipped with the ultra-low-voltage-noise SQUID-based self-balancing potentiometer circuit we used for the measurements in the paper. Commercial room-temperature preamplifiers typically have a voltage noise floor of several nV/√Hz (~1000 times larger than the voltage noise floor of our SQUID-based potentiometer), so measuring I-V curves of 20-mΩ SQUIDs with critical currents of a few μA requires extensive signal averaging. For this purpose we measured dV/dI vs I of the junctions using an ac technique with a lock-in amplifier. The dV/dI vs I data were then integrated to obtain the V vs I curves shown in fig. S1(A), acquired at T = 2.0 K for several different values of I_{flux}. Those I-V curves were fit with the square-root function (dashed lines), and a plot of I_c vs I_{flux} is shown in fig. S1(B). Figure S1(C) shows a plot of I_c vs temperature over the range 1.2 – 5.6 K. The values of I_c shown in this figure, as well as the extent of rounding of the I-V curves, are comparable to those obtained using the SQUID-based circuit. We conclude that the values of I_c measured in this work are not strongly attenuated by external interference. (Attempts to fit the data in fig. S1(A) with the Ivanchenko-Zil'berman function were unsuccessful due to small slope offsets in the data.)

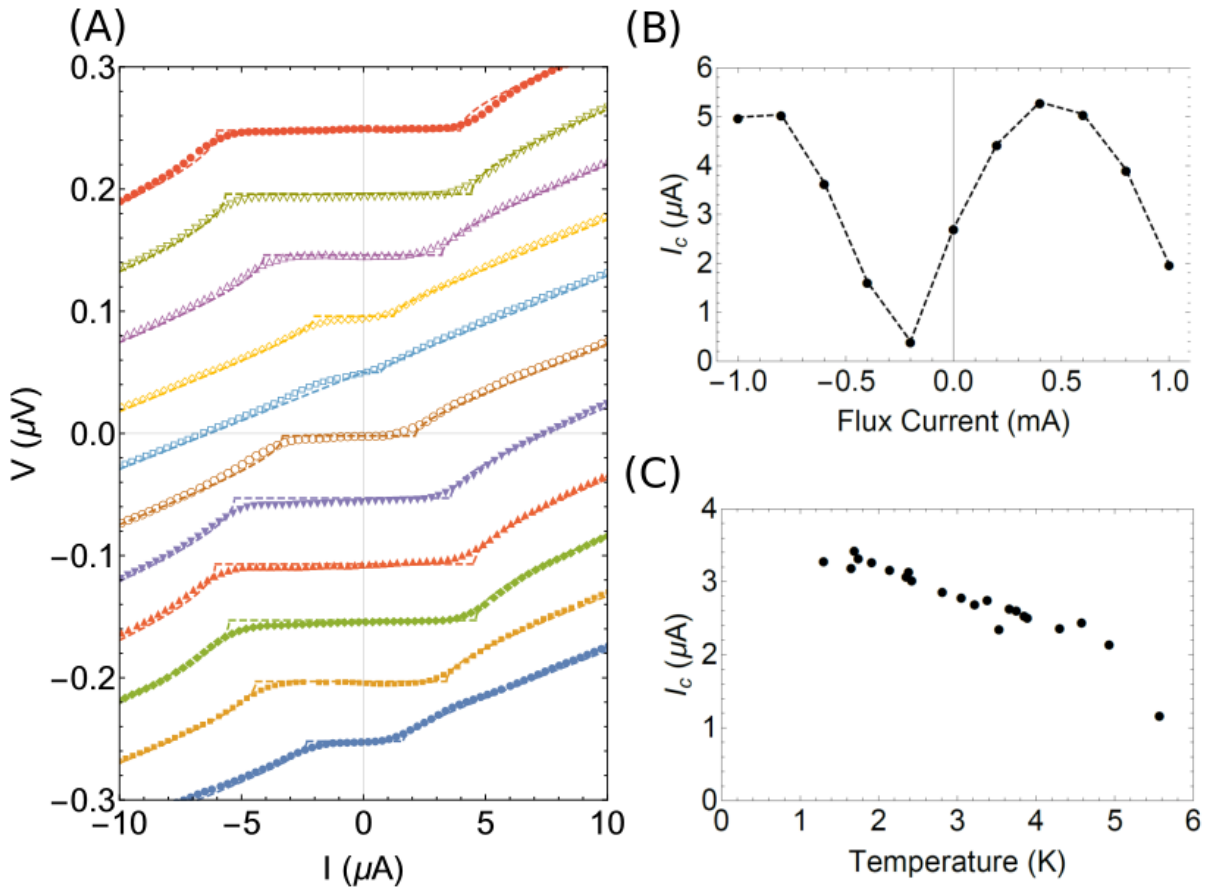

Fig. S1. Low-temperature measurements of sample 2A-1 with additional filtering. Critical current versus flux-line current and temperature for SQUID 2A-1 measured in a variable-temperature cryostat with heavily-filtered lines. (**A**) Data of dV/dI vs I were acquired at T = 2.0K using a lock-in amplifier technique, and were converted into I-V curves by numerical integration. The I-V curves display similar thermal rounding as the curves obtained using the SQUID-based self-balancing potentiometer circuit at 4.2 K, shown in Fig. 2(B). From top to bottom, each I-V curve corresponds to a different value of the applied flux current, starting at -1.0 mA and increasing by 0.2 mA for each successive curve. The curves are successively offset vertically by 0.25 μV for clarity. The dashed lines represent fits to the simple square-root function. (Fitting to the more accurate Ivanchenko-Zil'berman function was unsuccessful for a few of these curves due to the nonzero slope at zero applied current.) (**B**) Plot of critical current at 2.0 K versus I_{flux}. The dashed line is a guide the eye. (**C**) Measurements of critical current versus temperature, $I_c(T)$, with I_{flux} =0. While I_c increases with decreasing T, it is not substantially larger at 1-2 K than the previous measurements at 4.2 K. Temperature values above 4.2 K have large uncertainty due to extrapolation of the thermometer calibration curve.

Data from Additional Samples

Table I in the main text shows the fitting parameters obtained from seven SQUID samples. The data for sample 2A-4 are shown in Figs. 2 and 3 in the main text. The data for the other six samples are shown below in figs. S2-S7. All the data presented in figs. S2-S7 were obtained with the sample immersed in liquid helium at 4.2 K. Each figure consists of two parts: Panel (A) shows a 3D plot of I_c^{ave} vs I_{flux} and $\mu_0 H_{set}$, including data for both the upsweep and downsweep. Panel (B) shows a 2D plot of I_{c+} and I_{c-} vs I_{flux} for the two magnetic states, along with fits to standard SQUID theory (blue and yellow lines). The data in panels (A) were obtained from fitting the simple square-root function to the raw I-V data, whereas the data in panels (B) were obtained from fitting the more accurate Ivanchenko-Zil'berman function to the raw I-V data. Note the occasional errant or missing data point in the (B) panels – the latter due to the IZ fit not converging properly. Fortunately the frequency of such mishaps is low enough so as not to adversely affect the fits to the SQUID oscillations.

Figures S2-S4 show data for samples with the total number of [Pd/Co] bilayers, $2n$, in the central PMA SAF equal to 4, while figs. S5-S7 show data from samples with $2n = 6$. The critical currents are significantly smaller in the latter samples; nevertheless the sudden changes in the SQUID oscillations due to the changing magnetic states are still very clear.

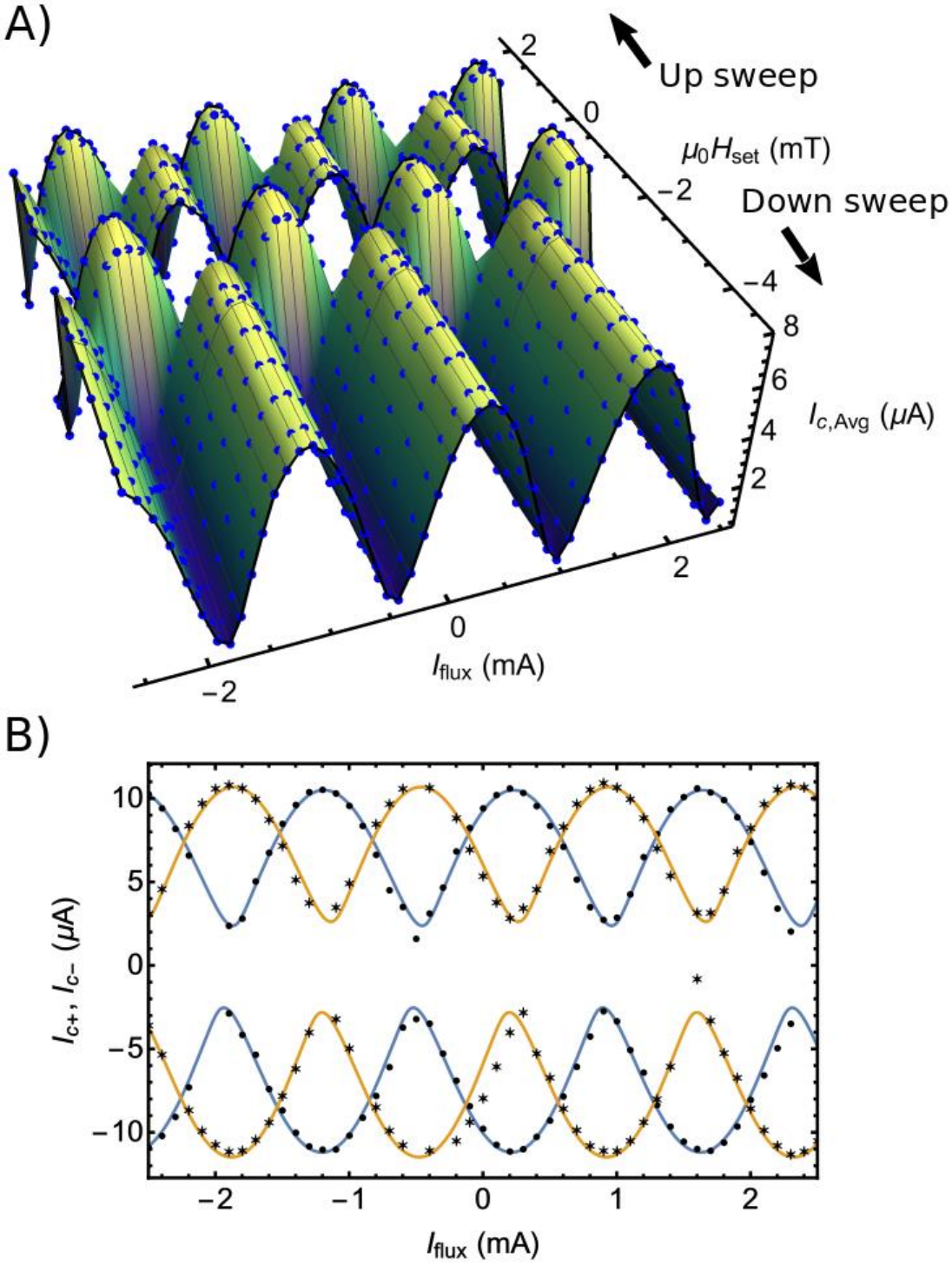

Fig. S2. Data from sample 2A-1. A) 3D plot of I_c^{ave} vs I_{flux} and $\mu_0 H_{set}$, showing both the upsweep and downsweep. **B**) 2D plot of I_{c+} and I_{c-} vs I_{flux} for the initial state (data: solid circles; fits: blue lines) and for the second magnetic state (data: stars; fits: yellow lines).

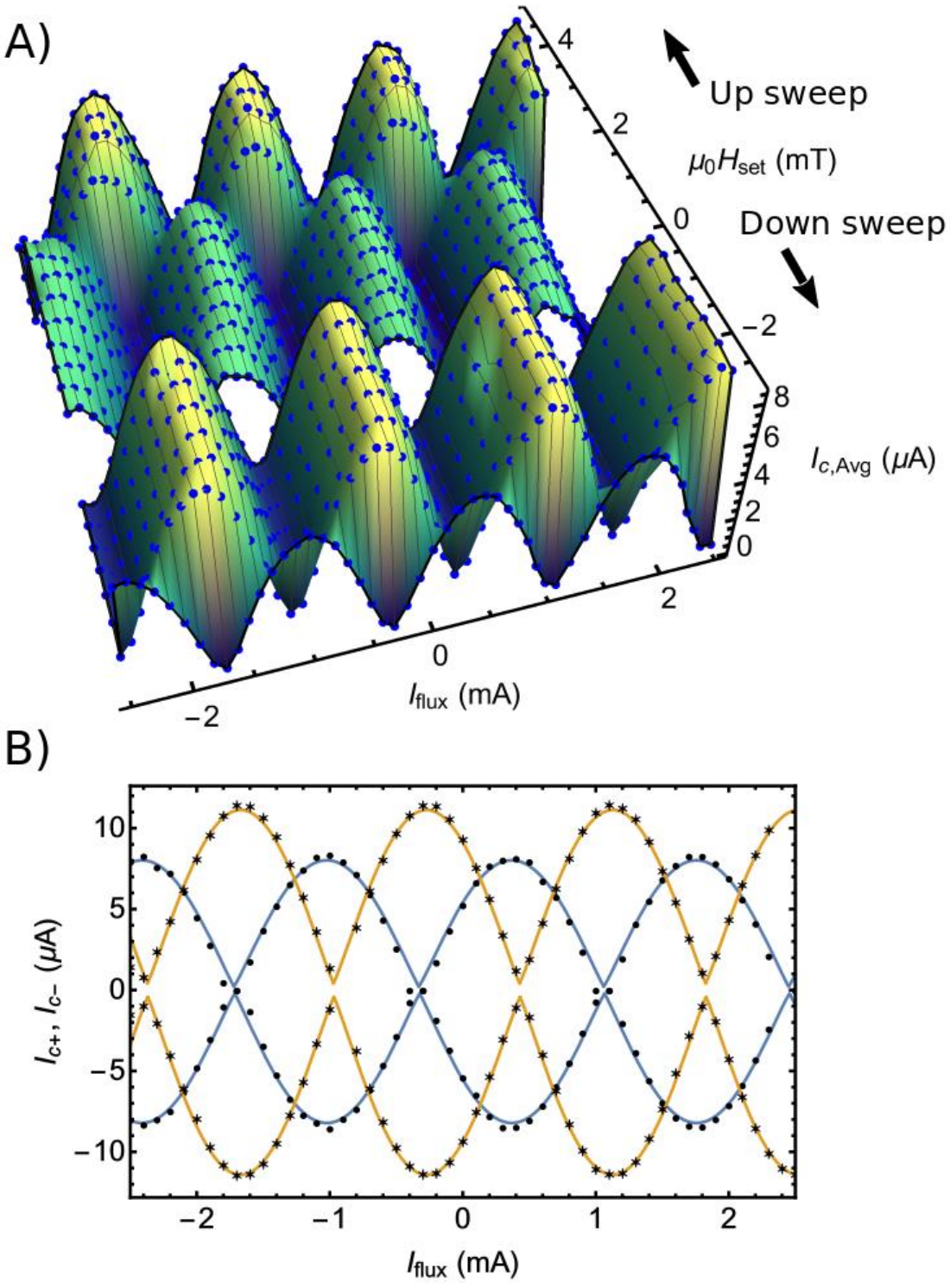

Fig. S3. Data from sample 2A-2. A) 3D plot of I_c^{ave} vs I_{flux} and $\mu_0 H_{set}$, showing both the upsweep and downsweep. **B**) 2D plot of I_{c+} and I_{c-} vs I_{flux} for the initial state (data: solid circles; fits: blue lines) and for the second magnetic state (data: stars; fits: yellow lines).

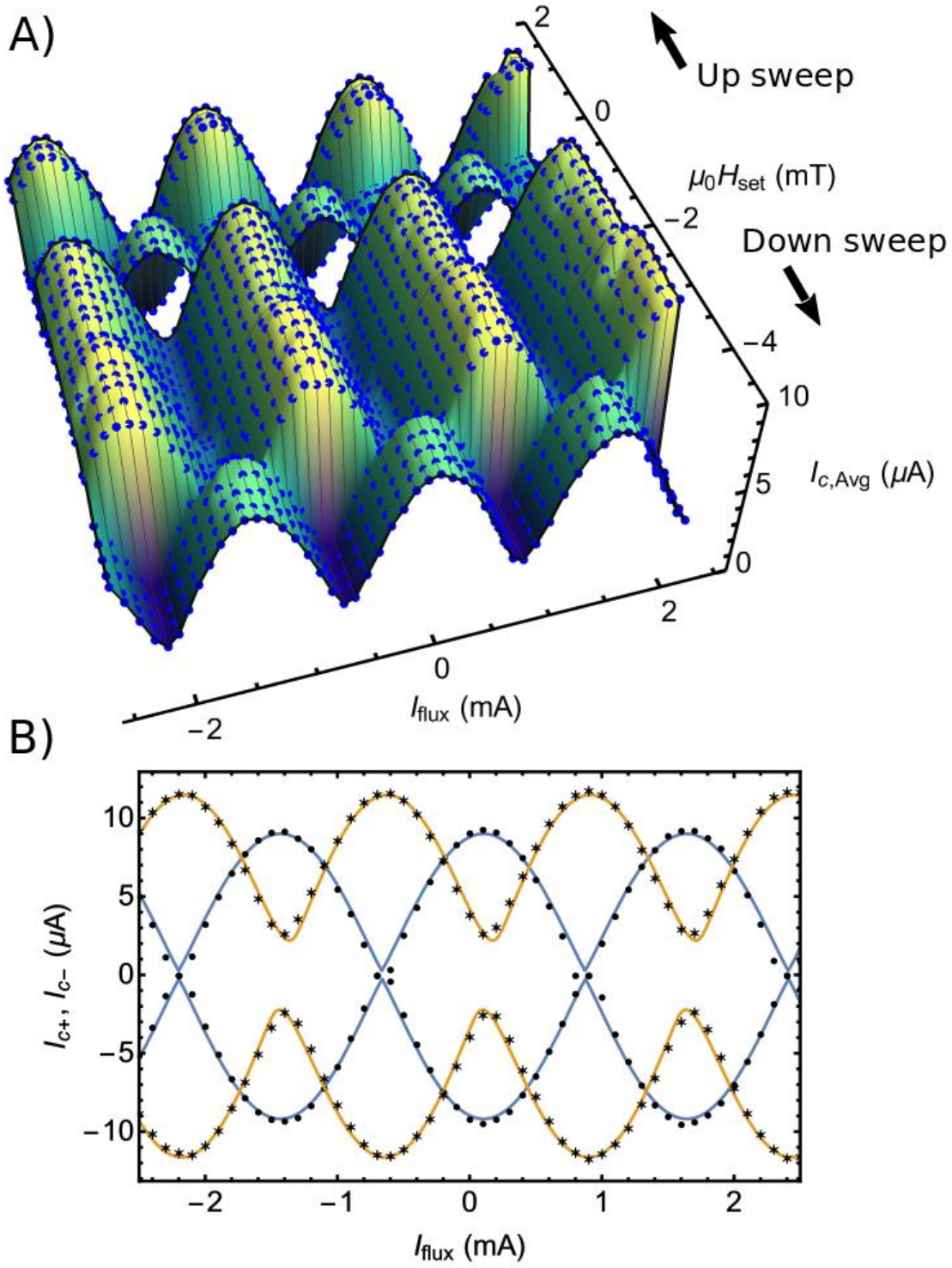

Fig. S4. Data from sample 2A-3. A) 3D plot of I_c^{ave} vs I_{flux} and $\mu_0 H_{set}$, showing both the upsweep and downsweep. **B**) 2D plot of I_{c+} and I_{c-} vs I_{flux} for the initial state (data: solid circles; fits: blue lines) and for the second magnetic state (data: stars; fits: yellow lines).

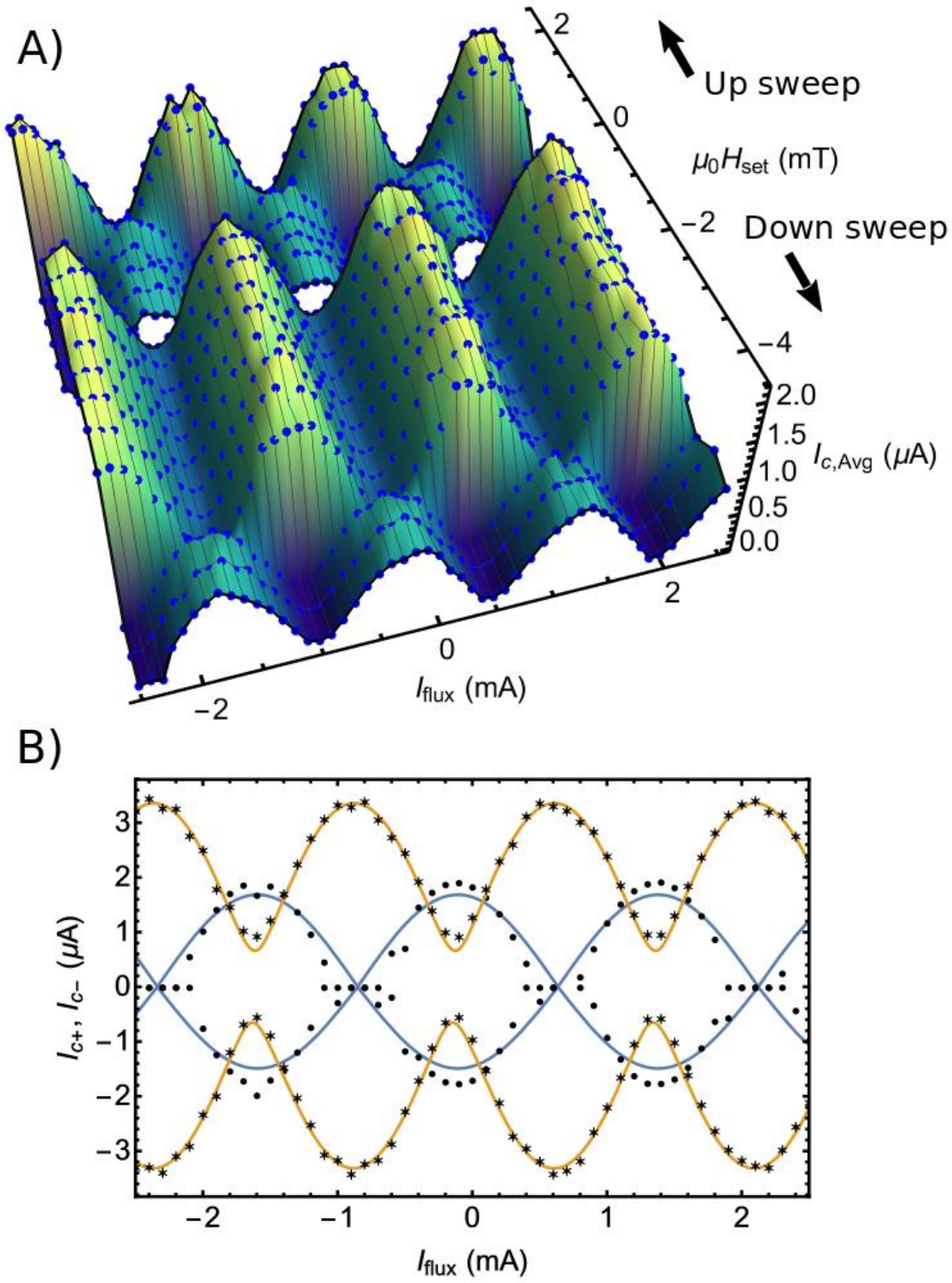

Fig. S5. Data from sample 3A-3. A) 3D plot of I_c^{ave} vs I_{flux} and $\mu_0 H_{set}$, showing both the upsweep and downsweep. **B**) 2D plot of I_{c+} and I_{c-} vs I_{flux} for the initial state (data: solid circles; fits: blue lines) and for the second magnetic state (data: stars; fits: yellow lines).

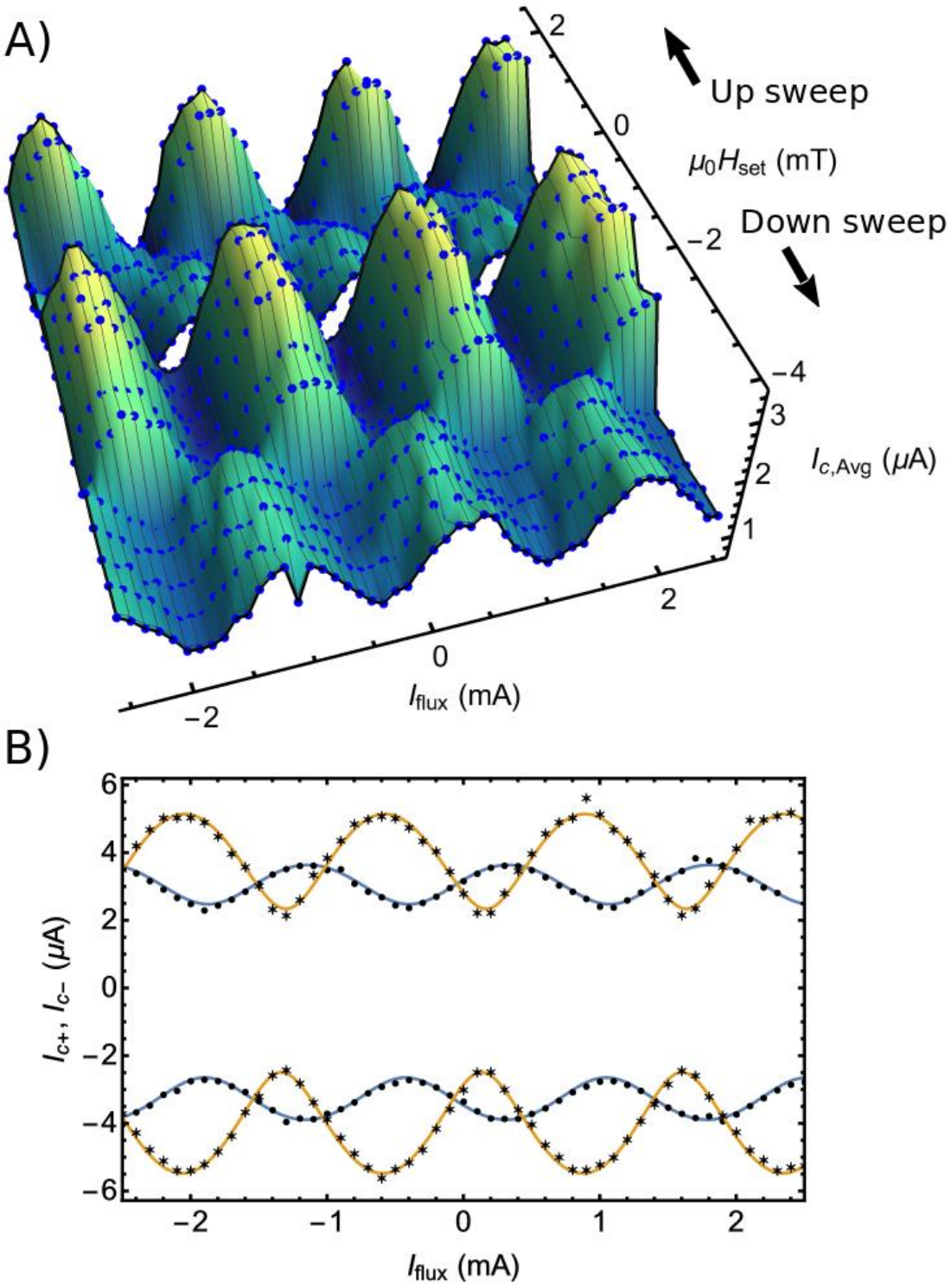

Fig. S6. Data from sample 4A-1. A) 3D plot of I_c^{ave} vs I_{flux} and $\mu_0 H_{set}$, showing both the upsweep and downsweep. **B**) 2D plot of I_{c+} and I_{c-} vs I_{flux} for the initial state (data: solid circles; fits: blue lines) and for the second magnetic state (data: stars; fits: yellow lines).

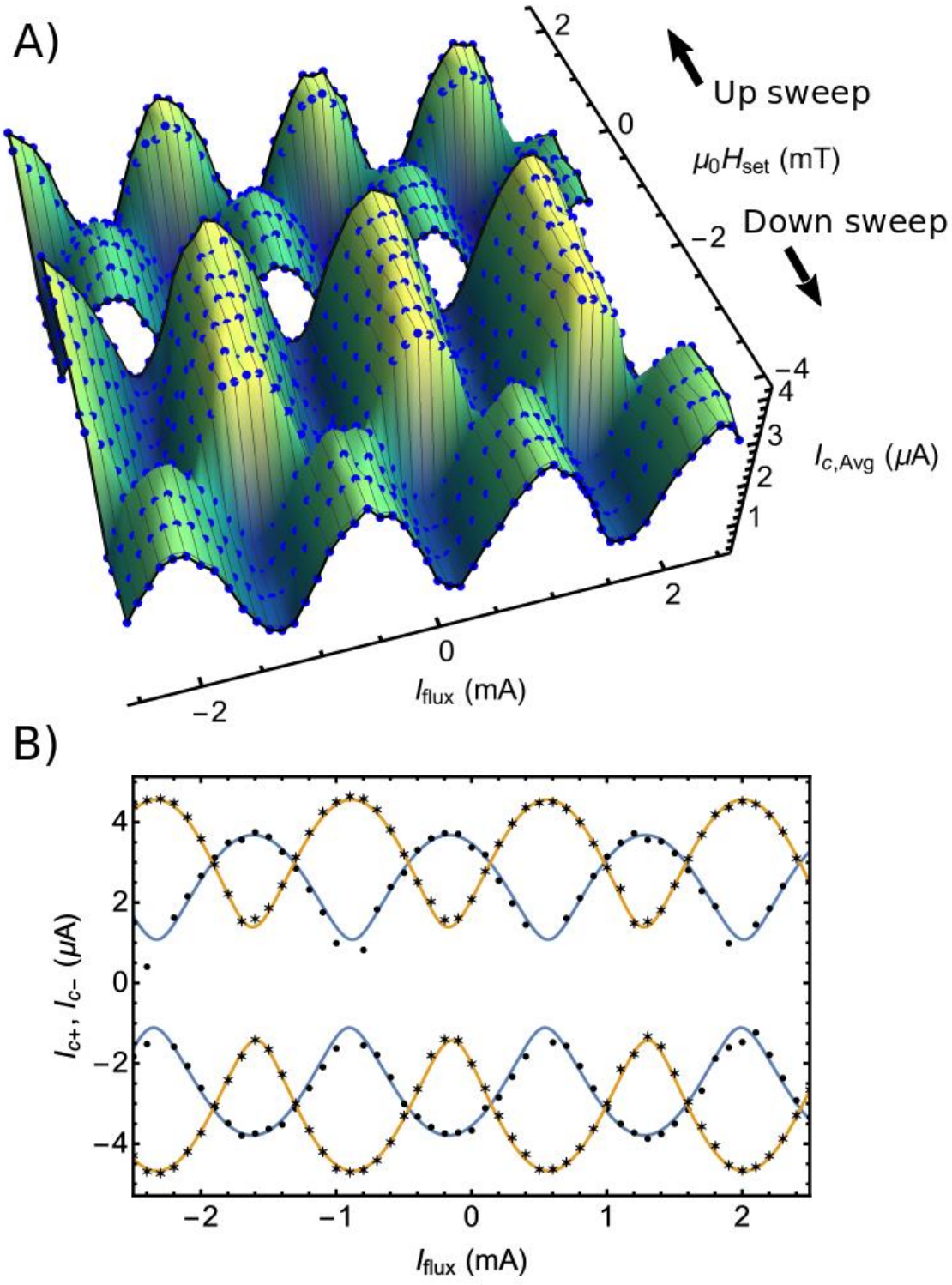

Fig. S7. Data from sample 4A-2. A) 3D plot of I_c^{ave} vs I_{flux} and $\mu_0 H_{set}$, showing both the upsweep and downsweep. **B**) 2D plot of I_{c+} and I_{c-} vs I_{flux} for the initial state (data: solid circles; fits: blue lines) and for the second magnetic state (data: stars; fits: yellow lines).